INFLUENCE OF TITANIUM CONTENT ON OXIDATION OF Nb-Ti ALLOYS (10, 20, 30 WT% Ti) IN THE TEMPERATURE RANGE 400°C-1300°C, AT OXYGEN PRESSURE 100 TORRS KINETICS AND OXYGEN DISSOLUTION STUDY

Christian Perrin

Laboratoire de Chimie des Solides, ERA CNRS N° 678, Université d'Orléans
45046 ORLEANS-CEDEX, FRANCE

Introduction

Oxidation of niobium as oxidation of titanium, at moderate oxygen pressures, leads to oxygen dissolution in the metal, with probably metallic oxide formation (suboxide) and oxide scale formation. Oxide scale is protective (parabolic stage) or porous (linear stage).
Although the inherent mechanical properties of niobium are attractive, the use of this metal in high temperature applications requires the addition of alloying elements, improving the poor oxidation resistance.
The oxidation of niobium base alloys has been studied by several authors [1-4] and among these alloys, the Nb-Ti alloys improve the oxidation resistance. The object of this work is to determine the effect of titanium content (10, 20, 30 wt% Ti) on protective properties of the oxide scale and on oxygen dissolution.

Experimental procedure

1. Materials

Three Nb-Ti alloys have been used in this investigation (10, 20, 30 wt% Ti). The chemical compositions of these alloys are tabulated in Table 1.

Table 1. Chemical compositions (ppm) or (wt%)

Elements	NbTi10	NbTi20	NbTi30
Ti	10.6%	20.2%	28.6%
Ta	35	20	<20
W	47	1720	1.59%
Mo	230	<20	20
Zr	91	<65	70
Fe	300	150	75
Si	700	110	120
Ni	28	<10	<10
Pb	31	< 5	< 5
Sn, Mn, Mg	<10	<10	<10
C	108	77	117
N	70	45	83
O	250	240	295

2. Preparation

The material used in this investigation was in form of small plates (thickness 1 mm). Rectangular specimens having a surface area of about 1. cm^2

were prepared by polishing through SiC paper, then were degreased, heated at 1000°C, at 10^{-8} torr oxygen pressure, at last were electrolytically polished and heated again in the same conditions.

3. Oxidation apparatus

The specimens were oxidized in the Setaram thermal microbalance at moderate pressure (100 torrs) and in the temperature range 350°C → 1300°C. The oxidation apparatus is illustrated in Figure 1.

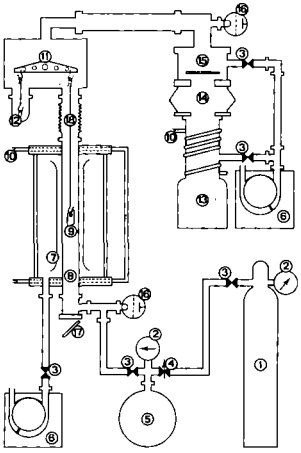

1) oxygen
2) manometer
3) valves
4) pressure control valve
5) oxygen reserve
6) fore-vacuum pump
7) high temperature furnace (tungsten resistor)
8) alumina tube
9) specimen
10) water cooling
11) Setaram microbalance
12) counterweight
13) oil diffusion pump
14) liquid nitrogen container
15) plate valve
16) ionisation gauges
17) glass window
18) quartz fiber

Figure 1 Schematic diagram of the oxidation apparatus

The specimen is placed into the alumina tube in the hot zone of furnace. It is suspended at the microbalance by a quartz fiber. The specimen is heated at the test temperature at low pressure (< 10^{-5} torr) then the gas is introduced at the experimental pressure. The weight-change measurements are obtained almost immediately, however the balances of pressure and temperature are realized after about five minutes.

Kinetics results

Weight-gains curves obtained, a comparison with niobium and titanium oxidation has been realized (data of Mollimard [5], Kofstad et al. [6]).
At 400-600°C, the alloys oxidation is parabolic. The behavior of the three alloys in this temperature range is comparable. A comparison with niobium and titanium oxidation is shown in Figure 2a.
In temperature range 600-800°C, the oxidation of the three alloys is always parabolic but a decreasing of the parabolic oxidation rate appears for NbTi20 alloy and essentially for NbTi30 alloy. This is illustrated in Figure 2b.
Above 800°C, the alloys oxidation initially follows an approximately parabolic law. Then a loss in protective behavior and an increase in the oxidation rate are observed (Figures 2c, d). The duration of the parabolic stage decreases with increasing temperature and with titanium content of alloys. The transition to linear oxidation takes place at shorter times the higher temperatures and depends also on the titanium content.

Figure 3 shows the dependency of parabolic and linear rate constants as a function of the temperature. The activation energy for the initial parabolic rate, below 800°C, for the three alloys, is an average activation energy cor-

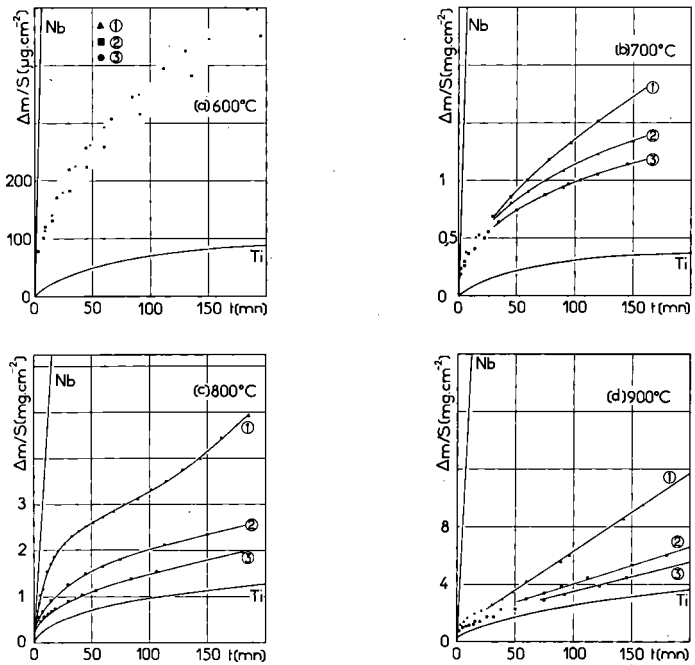

Figure 2 Oxidation of Nb-Ti alloys in 100 torrs O_2, weight-gains curves
Comparison with niobium and titanium oxidation [5] and [6]
(1) NbTi10 ; (2) NbTi20 ; (3) NbTi30

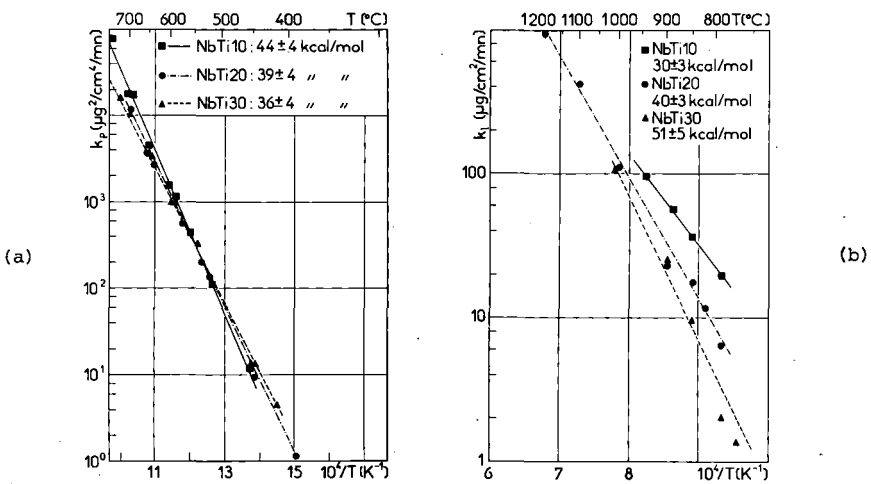

Figure 3 Oxidation of Nb-Ti alloys at 100 torrs O_2
Parabolic (a) and linear (b) rate constants as a function of 1/T

responding to oxide scale formation and oxygen dissolution.
In the pressure range 1-100 torrs, the pressure dependence has been also determined. It is very small, for the three alloys, suggesting a predominant diffusion mechanism.
In Figure 2, the behavior of niobium and titanium in the same conditions is compared to alloys behavior. In short, for all temperatures the niobium oxidation is the fastest. Below 800°C the niobium oxidation involves a pre-transition period (approximately parabolic) followed by a faster break-away oxidation. As for titanium, the alloys oxidation is parabolic in this temperature range. Above 800°C, the oxidation of niobium, titanium and alloys is linear, however the oxidation rate decreases with increasing titanium content.

Analysis

1. Metallographic examination

Oxidized specimens of Nb-Ti alloys have been prepared for metallographic examination. Typical cross sections of materials oxidized 4h at 100 torrs are shown in Figure 4. In both cases the general features of the microstructures are the same.

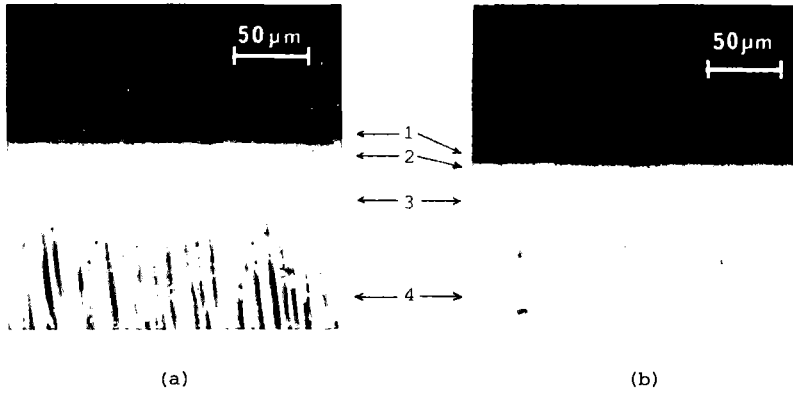

Figure 4 Cross-sections of Nb-Ti alloy specimens oxidized 4h, at 800°C in 100 mm O_2. (a) : NbTi20 ; (b) NbTi30
(1) : oxide scale (2) : external zone
(3) : hardened zone (4) : alloy

Below 800°C, an adherent, external oxide scale is observed. Under this external oxide is a layer of alloy satured with oxygen. For the same temperature, the hardened zone of NbTi10 alloys is the thickest.
Above 800°C, a porous, powdery oxide scale is formed. The thickness of hardened zone is observed when the decreasing of the parabolic rate appears, exclusively for NbTi20 and NbTi30 oxidation. This external zone has been observed in electron photomicrograph.

Below 800°C, for the three alloys, the thickness of the compact oxide scale has been measured through the cross-sections, in order to determine the oxygen quantity fixed in the oxide assumed to a mixture of Nb_2O_5 and TiO_2 oxides and also to determine the preponderant mechanism during the parabolic kinetics. The results are tabulated in Table 2. These results are compared with the weight-gains obtained in the thermogravimetric experiments. They show that dissolution is the preponderant mechanism.

Table 2. Oxide thickness (e), oxygen quantity fixed in Nb_2O_5 + TiO_2 oxides ($(\Delta m/S)_{ox.}$), weight-gains obtained by microgravimetric experiments ($(\Delta m/S)_t$), dissolved oxygen ($(\Delta m/S)_{diss.}$) as a function of alloys, oxidation temperature and time

Alloys	T (°C)	t (h)	$(\Delta m/S)_t$ (μg/cm²)	e_{oxide} (μm)	$(\Delta m/S)_{ox.}$ (μg/cm²)	$(\Delta m/S)_{diss.}$ $(\Delta m/S)_t - (\Delta m/S)_{ox.}$ (μg/cm²)
NbTi10	518	30	350	<< 1	<< 150	325 ± 25
	560	45	1090	< 1	< 150	980 ± 40
	590	31	1360	< 1	< 150	1250 ± 40
	605	8	715	< 1	< 150	620 ± 50
	650	8	1560	2.5 ± 0.5	375 ± 75	1180 ± 80
	700	7.33	2750	7.5 ± 0.5	1125 ± 75	1630 ± 80
	750	8	5700	21 ± 1	3150 ± 150	2550 ± 150
NbTi20	540	47	715	< 1	< 160	640 ± 40
	570	41.6	945	≃ 1	≃ 160	800 ± 40
	605	23.33	1080	> 1	> 160	920 ± 60
	640	8	1060	1.5 ± 0.5	230 ± 70	820 ± 60
	660	6	1050	1.5 ± 0.5	260 ± 60	790 ± 60
NbTi30	550	27	750	<< 1	<< 170	700 ± 50
	590	24	1000	< 1	< 170	890 ± 60
	605	8	770	< 1	< 170	650 ± 50
	650	8	1150	1.5 ± 0.5	260 ± 80	890 ± 80

2. X ray diffraction and electron microprobe analysis

The oxidized specimens and the cross sections have been observed by X ray diffraction and electron microprobe.

X ray diffraction analysis of the surface oxides shows a gradual transition from a poorly cristalline oxide, below 800°C, to the highly cristalline multiphase oxide product formed at higher temperature. The oxide is a mixture of $TiNb_2O_7$ [7], $Nb_2O_5\beta$ [8] and TiO_2 [9]. The amounts of these oxides change with the titanium content.

Between 500°C and 650°C, for NbTi10 and NbTi20 alloys, broad diffraction peaks could be assigned to a compound $(Nb\text{-}Ti)_4O$. The interplanar spacings obtained for NbTi20 specimens oxidized at 540°C, 605°C and for NbTi10 specimens oxidized at 518°C, 590°C are given in Table 3, the results are in fair agreement with the data given by Brauer for TaO_y [10]. The chemical formula of this suboxide found by Schönberg [11] and Steeb [12] is Ta_4O.

Above 700°C, for NbTi20 and NbTi30 alloys, new broad diffraction peaks which could not be positively identified are observed. These peaks correspond to either a tetragonal phase (a = 3.32 Å ; c = 3.62 Å), or an internal oxide precipitate in body centered cubic alloys. This phase appears in the alloy, in the hardened zone, at the oxide/alloy interface, when parabolic oxidation rate decreases.

Interplanar spacings obtained after oxide scraping, for NbTi30 specimen oxidized at 800°C and for NbTi20 specimen oxidized at 850°C are shown in Table 4.

Qualitative and quantitative microprobe analysis of cross sections of oxidized specimens show that the niobium and titanium contents in the oxide and the alloys remain constant during oxidation. The oxygen content in the phase which appears when parabolic oxidation rate decreases, has been estimated (about 30 at%) for NbTi20 and NbTi30.

Table 3. Interplanar spacings (d, Å) and intensities (I) obtained for NbTi20 specimens oxidized at 540°C, 605°C and for NbTi10 specimens oxidized at 518°C, 590°C.
Comparison with spacings given by Brauer for TaO_y [10]

NbTi20				NbTi10				TaO_y	
47h 540°C		23.3h 605°C		30h 518°C		31h 590°C		[10]	
d(Å)	I	d(Å)	I	d(Å)	I	d(Å)	I	d(Å)	(hkl) : I
2.40	10	2.41	10			2.43	10	2.411	(110) : 10
2.38		2.39		2,39	10	2.39		2.394	(101) :
2.29	3	2.25	f	2.29	4	2.29	5	2.287	(011) : 5
1.82	1	1.85	?	1.85	?	1.88	f	1.895	(200) : 4
1.60	f			1.60	?			1.627	(020) : 8
								1.594	(002) :
								1.415	(211) : 4
1.34	1	1.33	?			1.34	?	1.334	(112) : 6

Table 4. Interplanar spacings obtained for NbTi20 and NbTi30 oxidized specimens.
Comparison with calculated spacings of the tetragonal structure (a = 3.32 Å ; c = 3.62 Å)

NbTi30 800°C ; 25h	NbTi20 850°C ; 4h	Tetragonal structure a=3.32 Å ; c=3.62 Å	
d (Å)	d (Å)	d_{cal} (Å)	(hkl)
3.62	3.63	3.62	(001)
2.352	2.352	2.348	(110)
1.963	1.97	1.97	(111)
1.66	1.66	1.66	(200)

Microhardness study

1. Diffusion mechanism verification, below 700°C

Preliminary study shows that oxygen dissolution is the preponderant mechanism. A study of solid solution has been carried out by microhardness. The object of this study was to verify oxygen diffusion and also to determine parameters defining oxygen diffusion (limit concentration and diffusion coefficient of oxygen). The hardness penetration data may be utilized to calculate these parameters. Knoop and Vickers hardness traverses have been made on transverse sections of the oxidized specimens in order to measure the depth contamination (or diffusion) by oxygen. Some hardness penetration curves are given in Figure 5. If maximum depth of contamination is arbitrarily taken as the point where the hardness penetration curve reaches the base metal hardness value plus 50 VHN, the depth of contamination increases with decreasing titanium content. Moreover, the limit hardness (the hardness near the oxide/alloy interface) increases with increasing titanium content (about 1500 VHN for NbTi10, harder than 2200 for NbTi30).
Below 700°C, the parabolic oxidation of alloys results from simultaneous for-

mation of a compact scale and oxygen dissolution. A model involving the two mechanisms has been advanced by Wagner [13] and has been applied by Wallwork [14] and Debuigne [15] to the oxidation of zirconium.
This model assumes that oxygen diffuses inward through oxide and is consumed by oxide growth and oxygen dissolution at the metal/oxide interface. When oxygen dissolution is the preponderant mechanism, the oxide growth may be neglected and the oxygen concentration as a function of the depth is :

$$(c-c_o)/(c_s-c_o) = 1 - \mathrm{erf}(x/2\sqrt{Dt})$$

c, c_s, c_o : concentrations at a distance x from the surface, at the surface and in the core of the alloys,
D : diffusion coefficient independent on oxygen concentration,
t : oxidation time.

The following assumptions are necessary :
1) The diffusion coefficient does not vary with concentration,
2) The initial alloy/oxide boundary does not move.
If the hardness of alloys is assumed to vary linearly with oxygen concentration (assumption 3), hardness curve may be written :

$$(H-H_o)/(H_s-H_o) = 1 - \mathrm{erf}(x/2\sqrt{Dt})$$

H, H_s, H_o : hardness at a distance x from the surface, at the surface and in the core of the alloys,

The shape of our experimental curves (Figure 5) are complex and do not correspond to theoretical curves, also one or several assumptions are not probably verified.

Before verifying these assumptions, the diffusion of oxygen in alloys has been shown. For this, the depth of contamination expressed as the distance from the alloy surface to the point on the hardness traverse curve which is 50 points harder than the unreacted metal has been measured. The results are given in Table 5.
The depth of contamination x_{+50} varies with the square root of time when the oxygen diffuses in the alloy.

Indeed : $c = c(x_{+50}) = c_o+\varepsilon \rightarrow (c-c_o)/(c_s-c_o) = k = 1 - \mathrm{erf}(x_{+50}/2\sqrt{Dt})$

Therefore : $x_{+50}/2\sqrt{Dt} = k'$ and $x_{+50} = K'\sqrt{t}$

A contamination coefficient has been defined : $K = K'^2$
An Arrhenius type plot of the contamination rate ($K = x^2/t$) is shown in Figure 6. The activation energies for oxygen contamination in these alloys are calculated. They are comparable with the activation energies found for the global kinetics. Therefore the mechanism of dissolution is an oxygen diffusion mechanism and it is preponderant.

2. Hardness-concentration relation

It has been shown previously that one or several assumptions are not probably verified. The assumption 3, "the alloys hardness varies linearly with oxygen concentration", has been verified in measuring the areas included below microhardness curves and in showing that these areas are proportionnal to the dissolved oxygen quantity, for the three alloys and for all temperatures. The dissolved oxygen has been calculated in Table 2. These results are given in Table 6.

3. Diffusion coefficient

The assumption 2 is generally verified ; the oxide scale being almost always less thick than a few microns. The first assumption, "D independent on oxygen concentration" is not probably verified. Theoretical curves have been computed in considering D dependent on concentration. Different variation laws have been considered ; an exemple is shown in Figure 5 with the law :

Table 5. Experimental Weight-gains $(\Delta m/S)_t$, depth of contamination x_{+50}, contamination coefficient $K = (x_{+50})^2/t$ as a function of alloys, time and temperature of oxidation

Alloys	T (°C)	$10^4/T$ (K^{-1})	t (h)	$\Delta m/S$ ($\mu g/cm^2$)	x_{+50} (μm)	$(x_{+50})^2/t$ ($\mu m^2 \times h^{-1}$)
NbTi10	518	12.65	30	350	28 ± 2	26 ± 4
	560	12.	45	1090	62 ± 2	84 ± 4
	590	11.6	31	1360	75 ± 2	180 ± 10
	605	11.4	8	715	45 ± 2	247 ± 17
	650	10.83	8	1560	74 ± 2	675 ± 25
	700	10.28	7.33	2750	107 ± 2	1550 ± 50
	750	9.78	8	5700	127 ± 2	2030 ± 80
NbTi20	540	12.3	47	710	40 ± 2	34 ± 4
	570	11.86	41.6	950	54 ± 2	69 ± 4
	605	11.4	23.33	1080	57 ± 2	140 ± 10
	640	10.95	8	1060	54 ± 1	365 ± 15
	660	10.7	6	1050	51 ± 1	430 ± 15
NbTi30	550	12.15	27	740	35 ± 2	45 ± 5
	590	11.6	24	1000	48 ± 2	98 ± 10
	605	11.4	8	770	39 ± 2	185 ± 15
	650	10.8	8	1150	47 ± 2	280 ± 30
	700	10.28	6	1560	72 ± 2	880 ± 60
	800	9.3	4	2250	127 ± 2	4050 ±150

Table 6. Determination of oxygen quantity dissolved from areas included below microhardness curves.
Comparison with dissolved oxygen calculated in Table 2

Alloys	T (°C)	S (cm^2)	$k \times S = (\Delta m/S)_{diss.}$ k=19 ($\mu g/cm^2$)	$(\Delta m/S)_{diss.}$ (Table 2) ($\mu g/cm^2$)
NbTi10	518	18 ± 1	340 ± 20	325 ± 25
	560	51 ± 2	970 ± 40	980 ± 40
	590	61.5 ± 1.5	1170 ± 30	1250 ± 40
	605	34 ± 1	650 ± 20	620 ± 50
	650	66 ± 2	1260 ± 40	1180 ± 80
	700	93.5 ± 1.5	1770 ± 30	1630 ± 80
	750	123 ± 3	2340 ± 60	2550 ±150
NbTi20	540	31.5 ± 1.5	600 ± 30	640 ± 40
	570	43.5 ± 1.5	830 ± 30	800 ± 40
	605	48.5 ± 1.5	920 ± 30	920 ± 60
	640	46.5 ± 1.5	880 ± 30	820 ± 60
	660	43.5 ± 1.5	830 ± 30	790 ± 60
NbTi30	550	36 ± 2	680 ± 30	700 ± 50
	590	49.5 ± 1.5	940 ± 30	890 ± 60
	605	33.5 ± 1.5	640 ± 30	650 ± 50
	650	51.5 ± 1.5	980 ± 30	890 ± 80

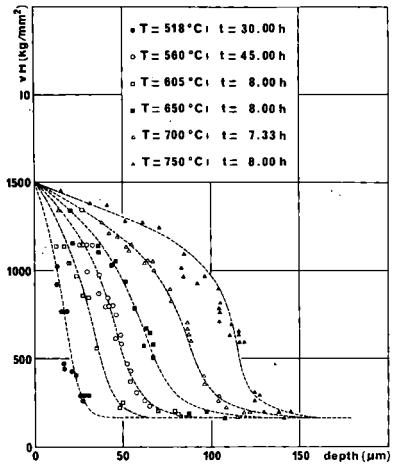

Figure 5 Experimental microhardness measurements (VH) NbTi10 alloys oxidized in 100 mm O_2 at 518°C → 750°C Theoretical curves calculated with $D(c) = D_o \exp(kc/c_s)$ $k \simeq 2$

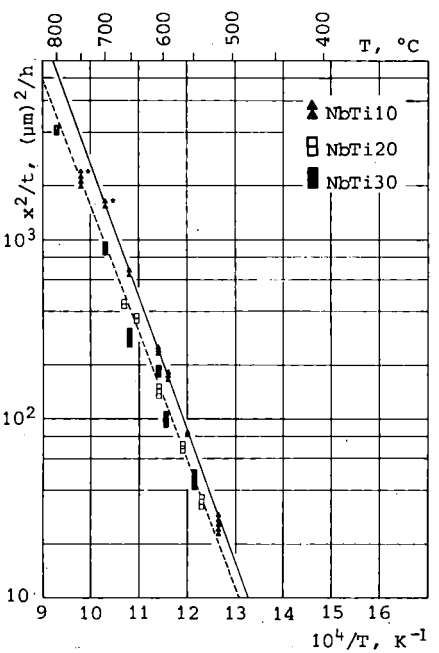

Figure 6 Dependency of contamination coefficients ($k = x^2_{+50}/t$) on temperature for Nb-Ti alloys

★ with interface correction

$$D = D_o \exp(kc/c_s)$$

The theoretical hardness curves obtained are in fair agreement with experimental hardness measurements. The shape of experimental curves may be therefore explained by a diffusion coefficient which varies with oxygen concentration.

4. Microhardness curves obtained above 700°C

The hardness curves obtained are complex because the assumption 2 is no more verified. The oxide thickness is important and the oxide/alloy interface moves as a function of time, moreover, the core of the alloy is contamined.

Discussion

This work enables to compare Nb-Ti alloys oxidation with niobium and titanium oxidation.
Between 450°C and 600°C, the niobium oxidation is the fastest because, for niobium, the nucleation of $Nb_2O_5\delta$ [16] and $Nb_2O_5\alpha$ [17] oxides is associated with the breakaway oxidation. For titanium as for Nb-Ti alloys, oxide scale is protective and the oxygen dissolution is the preponderant mechanism.
The solid solution has been studied by microprobe and microhardness technics. The oxygen concentration and the microhardness at the oxide/alloy interface increase with increasing titanium content (about 14 at% for NbTi10, 20 at% for NbTi30 alloys). The depth of oxygen contamination decreases with increasing titanium content and the diffusion coefficient varies with oxygen concentration.
Above 700°C, the parabolic oxidation rate decreases for NbTi20 and NbTi30 alloys. This decreasing corresponds to a new phase formed in the solid solution. Above 800°C, the oxidations of niobium, titanium and alloys are linear after an initial parabolic stage. As for titanium [18], the linear stage appears, for NbTi20 and NbTi30 alloys, after an outer layer of the alloys reaches a critical oxygen content which corresponds probably to the composition $(Nb\text{-}Ti)_3O$, composition $TiO_{0.35}$ for titanium.
In short, the titanium addition improves the poor oxidation resistance of niobium, especially below 800°C because the oxide scale formed has protective properties. The poorly cristalline oxide is a mixture of Nb_2O_5 and TiO_2 oxides.

References

1. P. Kofstad, H. Kjøllesdal and N. Norman : Technical Scientific Note, 3(1960).
2. B.B. Argent and B. Phelps : J. Less-Common Metals, 2(2,4)(1960), 181.
3. E.J. Felten : J. Less-Common Metals, 17(1969), 207.
4. R. Smith : J. Less-Common Metals, 2(1960).
5. D. Mollimard : Communication pers., Lab. de Chimie des Solides, Orléans.
6. P. Kofstad, K. Hauffe and H. Kjøllesdal : Acta Chem. Scand., 12(1958), 259.
7. R.S. Roth and L.W. Coughanour : J. Res. Nat. Bur. Stds., 55(4)(1955), 209.
8. R.P. Elliot : Trans. Am. Soc. Met., 52(1960), 990.
9. Swanson and Tatge : JC Fel. Reports NBS (1950).
10. G. Brauer, H. Müller and G. Khüner : J. Less-Common Metals, 4(1962), 533.
11. N. Schönberg : Acta Chem. Scand., 8(1954), 240.
12. S. Steeb : 2. Intern. Symp., Dresden, (1965).
13. C. Wagner and H.H. Von Baumbach : Z. Physik. Chem. Leipzig, 24(1934), 59.
14. G.R. Wallwork, W.W. Smeltzer and C.J. Rosa : Acta Met., 12(1964), 409.
15. J. Debuigne : Métaux Corrosion Industrie, (1967), 499.
16. L.K. Frevel and H.W. Rinn : Anal. Chem., 27(1955), 1329.
17. R.B. Hahn : J. Am. Chem. Soc., 73(1951), 5091.
18. P. Kofstad, P.B. Anderson and O.J. Krudtaa : J. Less-Common Metals, 3(1961), 89.